Size dependent ferromagnetism in cerium oxide (CeO_2) nanostructures independent of oxygen vacancies

2008 J. Phys.: Condens. Matter 20 165201

(http://iopscience.iop.org/0953-8984/20/16/165201)

J. Phys.: Condens. Matter **20** (2008) 165201 (5pp) doi:10.1088/0953-8984/20/16/165201

Size dependent ferromagnetism in cerium oxide (CeO_2) nanostructures independent of oxygen vacancies

Yinglin Liu[1], **Zainovia Lockman**[2], **Azizan Aziz**[2] **and Judith MacManus-Driscoll**[1,3]

[1] Department of Materials Science and Metallurgy, University of Cambridge, Pembroke Street, Cambridge CB2 3QZ, UK
[2] School of Materials and Mineral Resources Engineering, Engineering Campus, Universiti Sains Malaysia, 14300 Nibong Tebal, Penang, Malaysia

E-mail: jld35@cam.ac.uk

Received 1 December 2007, in final form 3 December 2007
Published 31 March 2008
Online at stacks.iop.org/JPhysCM/20/165201

Abstract
Nanosized cerium oxide (CeO_2) powders of different sizes were synthesized through homogeneous precipitation. Ferromagnetism was observed *only* in sub-20 nm powders. Ferromagnetic transition temperatures above room temperature and saturation magnetization values of 0.023 μ_B per CeO_2 formula unit were measured. Chemical analysis of the powders showed that trace ferromagnetic impurities could not be responsible for the magnetic signals. Carefully controlled coulometric cyclic annealing studies combined with photoluminescence measurements showed that oxygen vacancies do not mediate the ferromagnetism in the samples.

Dilute magnetic semiconductors (DMS) have drawn considerable attention due to their potential use in spintronics. It is generally accepted that magnetic order in a semiconductor requires a few per cent of transition metal ion dopants that have partially filled shells of d or f electrons to mediate ferromagnetism [1–3]. Recently, Venkatesan *et al* reported room temperature ferromagnetism in undoped hafnium dioxide thin films [4]. This work is intriguing because neither Hf^{4+} nor O^{2-} are magnetic ions and the d and f shells of the Hf^{4+} ion are either empty or full. Oxygen vacancy defects were assumed to give rise to the ferromagnetism [4, 5]. First-principles band structure calculations [6] indicate that the ferromagnetism may arise from hafnium vacancies (V_{Hf}).

Besides HfO_2, several observations of ferromagnetism above room temperature have been reported in systems with no unpaired d or f electrons, including undoped TiO_2, In_2O_3 thin films [7, 8], amorphous $HfAlO_x$ thin films [9], Cu-doped TiO_2 [10], undoped $TiO_{2-\delta}$ films [11], Ti-doped ZnO nanoclusters [12], proton-irradiated graphite [13], and CaB_6 [14]. Sundaresan *et al* also reported the observation of ferromagnetism at room temperature in nanoparticles of non-magnetic oxides such as CeO_2, Al_2O_3, ZnO, In_2O_3 and SnO_2, but did not show size dependency effects [15]. Recent reports on other magnetic ion-doped ferromagnetic oxides (e.g. Co-doped ZnO, Cr-doped ZnO and Ni-doped SnO_2 nanoparticle samples) [16–19] also indicate a link between defects and ferromagnetism.

The aim of this work was to further probe the relation between defects and ferromagnetism in an undoped oxide. A d^0 oxide, CeO_2, was studied in nanopowder form. For establishing the existence and nature of ferromagnetism in d^0 oxides, there are three principal advantages of using a nanostructured powder sample over thin film or bulk:

(1) nanopowders can be fabricated in much larger volumes than thin films. This means it is possible to quantitatively measure the concentration of any impurity magnetic elements present, and therefore, be certain of whether they are or are not responsible for the observed ferromagnetism;
(2) nanopowders have a much greater surface to volume ratio than bulk, so the fraction of surface defects is enhanced;
(3) it is possible to modify the particle size and therefore the surface defect relative to bulk fraction by a large amount.

Powders were made by homogeneous precipitation. 4 M NH_4OH or NaOH was added drop-wise to a stirred solution

[3] Author to whom any correspondence should be addressed.

Table 1. Samples synthesized from different solvents and summary of their magnetic properties.

Sample label	Solvent	Morphology	Size	Calculated SA/V ratio (nm^{-1})	As deposited	Air anneal	Reducing anneal
A	Pure water	Sphere	200–500 nm	0.03	Paramagnetic	Diamagnetic	Diamagnetic
B	50%ethanol + 50%water	Sphere	5–20 nm	0.3	Ferromagnetic, $T_c = 275$ K	Diamagnetic	Diamagnetic
C	50%PEG + 50%water	Needle	<1 nm thick 2–20 nm long	4.4	Ferromagnetic, $T_c > 300$ K	Diamagnetic	Diamagnetic

of 0.2 mol $Ce(NO_3)_3{\cdot}6H_2O$ dissolved in different solvents, following by heating at 60 °C until the pH of the solution was stabilized at >11. Three kinds of solvents were used, include 100% pure water, a 50% ethanol/50% water mixture and a 50% polyethylene glycol (PEG-1500)/50% water mixture. The precipitated powders were centrifuged, cleaned, dried and labeled as powders A, B and C, as listed in table 1. Non-magnetic tweezers and containers were used to avoid contamination of the powders during the growth and in subsequent measurements.

Field emission scanning electron microscopy (FE-SEM) and transmission electron microscopy (TEM) were used to investigate the shape and size of the powders. X-ray diffraction (XRD) (Cu Kα radiation) and Raman spectroscopy (488 nm Ar^+ laser) were used for phase identification. Magnetic properties were measured using a superconducting quantum interference device (SQUID). Post-anneals on the powders were conducted using a coulometric titration annealing system [16, 20]. The coulometric titration system allows for a very precise measurement of oxygen and provides a much more reducing environment than is provided by flowing Ar gas. Photoluminescence (PL) spectra were measured using an Accent RPM 2000 compound semiconductor PL system with laser wavelength of 266 nm.

As shown in figure 1 and table 1, the solvent played an important role in determining the powder sizes and morphologies. Powders A and B were composed of rounded particles of size 200–500 nm and 5–20 nm, respectively (figures 1(a) and (b)). By adding PEG to the solution, the shape of powder C was changed from spheres to needles. The needles were <1 nm thick and were 2–20 nm long (figure 1(c)). Both the XRD patterns and Raman spectra indicate the formation of pure CeO_2.

The magnetic properties of samples of reference commercial CeO_2 powder as well as the starting $Ce(NO_3)_3{\cdot}6H_2O$ and PEG surfactant were also measured. None of the chemicals showed magnetic signals from 10–300 K.

The magnetic properties of the CeO_2 powders are shown in figures 1(d)–(f) and table 1. From 10–300 K, the 200+ nm sized powder A was paramagnetic (figure 1(d)). Since bulk CeO_2 is diamagnetic, the paramagnetism likely originates from a small amount of remaining paramagnetic Ce^{3+} in the powder or from the sample holder. After subtracting the linear background, no signal remained.

At 300 K, nanoparticle powder B did not show ferromagnetism after linear background subtraction (figure 1(e)). However, at 200 K and below hysteresis loops were observed, indicative of ferromagnetism. The zero field cooled–field cooled (ZFC–FC) M–T curves measured at 500 Oe (inset of figure 1(e)) showed no superparamagnetic characteristics such as irreversibility or the presence of a cusp. The T_c of the powder was estimated to be 275 K and the sharp transition was indicative of spontaneous magnetic ordering.

M–H curves for nanoneedle sample C at different temperatures after linear background subtraction (figure 1(f)) showed hysteresis loops from 10 to 300 K. The inset of figure 1(f) shows a magnified part of the 300 K loop. The powder has a coercivity (H_c) of 73 Oe and 8% remnant magnetization (M_R). The values are slightly larger than reported on undoped HfO_2 films (20–50 Oe and 2–5% respectively) [5]. The saturation magnetization (M_S) is about 0.08 emu g^{-1} or 0.023 μ_B per CeO_2 formula unit and is around half the value of the HfO_2 films [4, 5]. However, the value is three orders of magnitude larger than annealed micron-sized HfO_2 powders [5].

The temperature dependent M_S and H_C curves for powder C are plotted in figure 2. M_S is fairly flat with temperature, indicating that $T_c > 300$ K. H_C decreases gradually with temperature, similar to what is observed in Co-doped ZnO nanocrystals [21] and Cr-doped CdTe crystals [22].

To exclude the possibility of impurities giving rise to the ferromagnetism, inductively coupled plasma-mass spectrometry (ICP-MS) was measured for powders A and B. ICP-MS is a powerful tool for trace and ultra-trace elemental analysis to one part in 10^9. Table 2 lists the Fe, Co and Ni concentrations in powders A and B together with the calculated magnetization values assuming the impurities are in their elemental form.

For powder B, assuming the Fe, Co, Ni were all in metallic state, and using the moment per atom for them of 2.22, 1.72 and 0.606 μ_B at 0 K, respectively [23], the sum of the M_S values is 0.006 emu g^{-1}, more than an order of magnitude lower than the measured value for powder B of 0.096 emu g^{-1}. Hence, the impurities are not responsible for the ferromagnetism.

The ICP results for powder A further confirm that the magnetic signal is not from impurities. The sum of calculated M_S values for the metallic impurities in powder A is 0.0186 emu g^{-1}. For 4 mg of the measured powder, a signal of 7.5×10^{-5} emu should be measured. This value is well within the sensitivity limit of the SQUID magnetometer and yet no ferromagnetic signal was measured. Hence, some or all of the impurities must be in the form of non-ferromagnetic oxides. This is unsurprising since non-vacuum wet chemical routes as used here provide a relatively oxidizing environment.

The surface area to volume ratio (SA/V) ratios calculated for the three powders are 0.03 nm^{-1} (A), 0.3 nm^{-1} (B) and

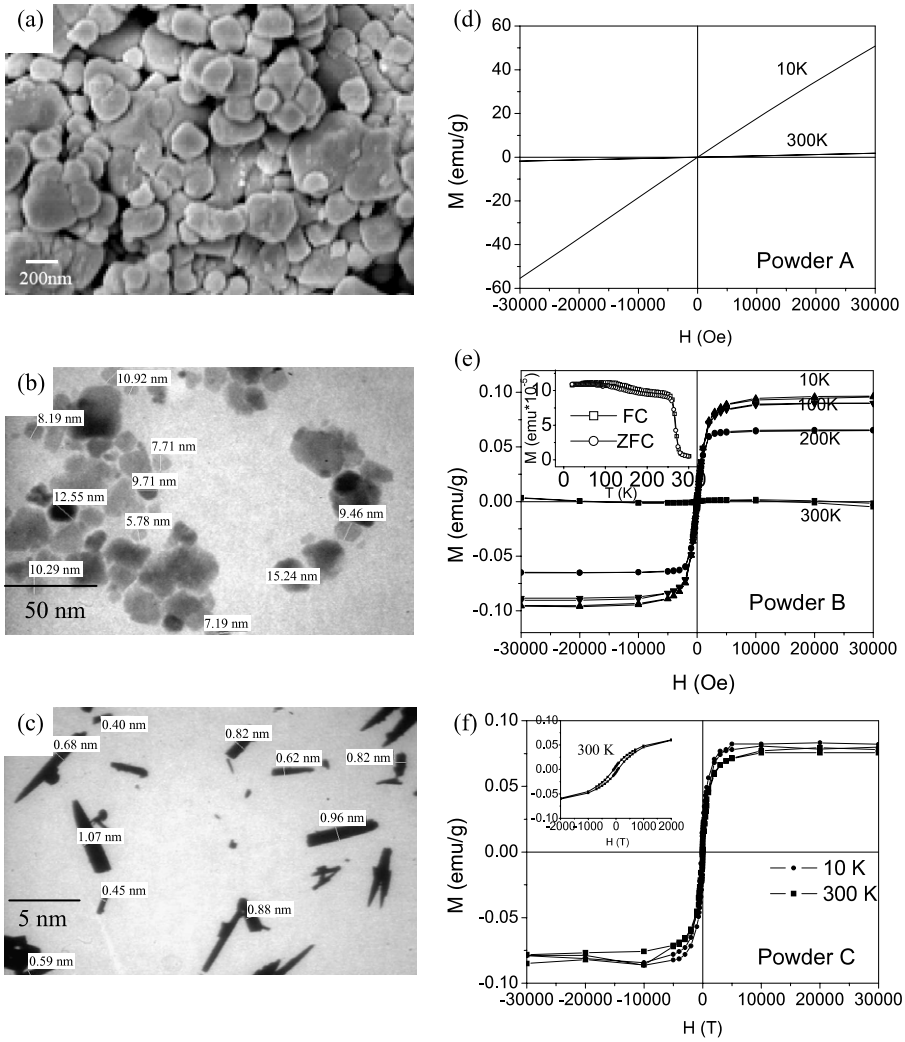

Figure 1. FE-SEM image of powder A grown in pure water (a) and TEM images of powders B (b) and C (c) grown from 50% ethanol 50% water and 50% PEG 50% water and their corresponding M–H curves for powders A (d), B (e) and C (f), measured at different temperatures after subtracting a linear background. The inset of (e) shows the ZFC–FC curves for powder B measured at 500 Oe. The inset of (f) is the enlarged loop of the M–H curve for powder C measured at 300 K.

Table 2. Concentration of magnetic impurities in CeO_2 powders measured by ICP-MS and calculated magnetization values assuming the impurity elements are in their metallic states.

	Powder A 200–500 nm particles (non-magnetic)			Powder B 5–20 nm nanopowders (magnetic)		
Impurity	Concentration (mg kg^{-1})	Calculated magnetization value from impurity (10^{-3} emu g^{-1}) 0 K	Magnetization value measured by SQUID (10^{-3} emu g^{-1}) at 10 K	Concentration (mg kg^{-1})	Calculated magnetization value from impurity (10^{-3} emu g^{-1}) 0 k	Magnetization value measured by SQUID (10^{-3} emu g^{-1}) at 10 K
Iron	81.8	18	—	9.8	2.2	—
Cobalt	2.6	0.4	—	22.4	3.7	—
Nickel	<2.2	0.1	—	<5.6	<0.3	—
Total	—	18.5	0	—	6.2	96

4.4 nm^{-1} (C), respectively (table 1). This assumes 200 nm spheres (A), 20 nm spheres (B) and 5 nm × 1 nm × 1 nm needles (C). The SA/V values increased by an order of magnitude from A to B and from B to C.

Oxygen vacancies have been speculated to be the cause of ferromagnetism in undoped oxides [4, 5]. To probe this, post-anneals were conducted either in air or in a very reducing environment, $p_{O_2} \sim 10^{-11}$ atm at 600 °C for 3 h. The

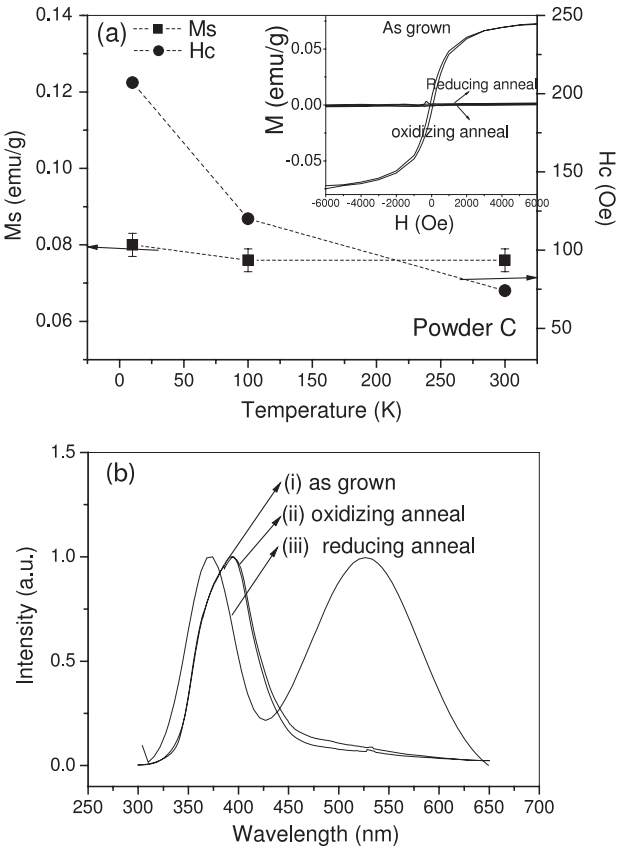

Figure 2. (a) The temperature dependent saturation magnetization (M_S) and coercive field (H_c) for nanoneedle powder C. Dashed lines are guides to the eye. The inset of (a) shows the M–H curves at 300 K (after subtracting a linear background) for nanoneedle powder C, as-grown, after an oxidizing anneal, and finally after a reducing anneal. (b) Normalized room temperature PL spectra excited by a 266 nm laser for sample C, as deposited (i), after an oxidizing anneal (ii), and after a reducing anneal (iii).

oxygen diffusion coefficient in CeO_2 at the anneal temperature is $<10^{-13}$ m^2 s^{-1} [24]. After 3 h, the estimated diffusion distance is <33 μm, which is much larger than the powder sizes, hence sufficient time was allowed for oxygen content change across the *whole* powder.

The resulting magnetic properties after these anneals are shown in table 1. It is observed that regardless of the annealing environment, no ferromagnetic signal was observed for any of the powders. The hysteresis data for air annealed and then reducing annealed powder C (inset to figure 2(a)) also shows this clearly.

Figure 2(b) shows the normalized PL spectra for powder C in the as-grown state, after oxidizing annealing, and after reducing anneal. The as-grown powder (i) shows a strong peak in the violet/blue range (at around 394 nm) which is attributable to charge transitions from the 4f band to the valence band of CeO_2 [25]. The spectrum is almost identical after oxidizing annealing (ii). After reducing annealing (iii), the violet/blue emission peak shifts to lower wavelength (around 370 nm). This shift is related to the change of the Ce ion valence from 4^+ to 3^+ [26, 27] and is consistent with the reducing annealing conditions. An additional broad emission band associated with oxygen vacancy defects is also present at around 550 nm [28, 29]. This peak is, again, consistent with the reducing anneal.

Since the reducing annealed sample C does not exhibit ferromagnetism, the PL results prove that oxygen vacancies are not responsible for the ferromagnetism observed in our size-controlled CeO_2 nanostructures. Ferromagnetic oxide impurities like Fe_3O_4 also play no role because the cyclic annealing experiments did not alter the magnetic state of the powder, even though the conditions would cause a phase change from oxidized (e.g. Fe_2O_3) to reduced (e.g. Fe_3O_4) material. On the other hand, a potential defect which would decrease in concentration with annealing is a cation surface defect state. These are commonly found in oxides, e.g. in MgO [30].

In summary, room temperature ferromagnetism was observed in sub-20 nm sized CeO_2 nanopowders. Chemical analysis by ICP showed that magnetic signals could not possibly originate from magnetic impurities. Controlled annealing studies to modify oxygen stoichiometry combined with PL showed that ferromagnetism is not linked to oxygen vacancies.

Acknowledgments

The authors thank Dr M Venkatesan, Physics Department, Trinity College, for the ICP measurement. Yinglin Liu and J L MacManus-Driscoll and the University of Cambridge acknowledge the EU Marie Curie Excellence Grant, NanoFen, EXT-014156 for provision of funding.

References

[1] Dietl T, Ohno H, Matsukura F, Cibert J and Ferrand D 2000 *Science* **287** 1019
[2] Matsumoto Y, Murakami M, Shono T, Hasegawa T, Fukumura T, Kawasaki M, Ahmet P, Chikyow T, Koshihara S and Koinuma H 2001 *Science* **291** 854
[3] Ohno H 1998 *Science* **281** 951
[4] Venkatesan M, Fitzgerald C B and Coey J M D 2004 *Nature* **430** 630
[5] Coey J M D, Venkatesan M, Stamenov P, Fitzgerald C B and Dorneles L S 2005 *Phys. Rev.* B **72** 024450
[6] Das Pemmaraju C and Sanvito S 2005 *Phys. Rev. Lett.* **94** 217205
[7] Hong N H, Sakai J, Poirot N and Brize V 2006 *Phys. Rev.* B **73** 132404
[8] Hong N H, Sakai J and Gervais F 2007 *J. Magn. Magn. Mater.* **316** 214
[9] Qiu X Y, Liu Q M, Gao F, Lu L Y and Liu J M 2006 *Appl. Phys. Lett.* **89** 242504
[10] Duhalde S, Vignolo M F, Golmar F, Chiliotte C, Torres C E R, Errico L A, Cabrera A F, Renteria M, Sanchez F H and Weissmann M 2005 *Phys. Rev.* B **72** 161313
[11] Yoon S D, Chen Y, Yang A, Goodrich T L, Zuo X, Arena D A, Ziemer K, Vittoria C and Harris V G 2006 *J. Physique* **18** L355
[12] Antony J, Pendyala S, McCready D E, Engelhard M H, Meyer D, Sharma A and Qiang Y 2006 *IEEE Trans. Magn.* **42** 2697
[13] Han K H, Spemann D, Esquinazi P, Hohne R, Riede V and Butz T 2003 *Adv. Mater.* **15** 1719

[14] Dorneles L S, Venkatesan M, Moliner M, Lunney J G and Coey J M D 2004 *Appl. Phys. Lett.* **85** 6377
[15] Sundaresan A, Bhargavi R, Rangarajan N, Siddesh U and Rao C N R 2006 *Phys. Rev.* B **74** 161306
[16] Khare N, Kappers M J, Wei M, Blamire M G and MacManus-Driscoll J L 2006 *Adv. Mater.* **18** 1449
[17] Archer P I and Gamelin D R 2006 *J. Appl. Phys.* **99** 08M107
[18] Hong N H, Sakai J, Huong N T, Poirot N and Ruyter A 2005 *Phys. Rev.* B **72** 045336
[19] Schwartz D A and Gamelin D R 2004 *Adv. Mater.* **16** 2115
[20] Porat O and Riess I 1994 *J. Electrochem. Soc.* **141** 1533
[21] Schwartz D A, Norberg N S, Nguyen Q P, Parker J M and Gamelin D R 2003 *J. Am. Chem. Soc.* **125** 13205
[22] Ko K Y and Blamire M G 2006 *Appl. Phys. Lett.* **88** 172101
[23] Kittel C 2002 *Introduction to Solid State Physics* 7th edn (New York: Wiley)
[24] Kamiya M, Shimada E, Ikuma Y, Komatsu M and Haneda H 2000 *J. Electrochem. Soc.* **147** 1222
[25] Gao F, Li G H, Zhang J H, Qin F G, Yao Z Y, Liu Z K, Wang Z G and Lin L Y 2001 *Chin. Phys. Lett.* **18** 443
[26] Chai C L, Yang S Y, Liu Z K, Liao M Y, Chen N F and Wang Z G 2001 *Chin. Sci. Bull.* **46** 2046
[27] Yu S H, Colfen H and Fischer A 2004 *Colloids Surf.* A **243** 49
[28] Morshed A H, Moussa M E, Bedair S M, Leonard R, Liu S X and ElMasry N 1997 *Appl. Phys. Lett.* **70** 1647
[29] Maensiri S, Masingboon C, Laokul P, Jareonboon W, Promarak V, Anderson P L and Seraphin S 2007 *Cryst. Growth Des.* **7** 950
[30] Kingery W D 1960 *Introduction to Ceramics* (New York: Wiley)